Pak. J. Bot., 57(6): DOI: http://dx.doi.org/10.30848/PJB2025-6(16)

CERIUM NITROGEN CO-DOPED CARBON DOTS PROMOTE ROOT GROWTH OF *ARABIDOPSIS THALIANA* VIA AUXIN SYNTHESIS AND TRANSPORT

TING MU[1,2], CHEN ZHAO[1,2], XIAOLEI WANG[1,2], CHENG SUN[1,2], CHANG HE[1,2] AND RONG HAN[1,2*]

[1]*College of Life Science, Shanxi Normal University, Taiyuan, Shanxi, 030000, People's Republic of China*
[2]*Higher Education Key Laboratory of Plant Molecular and Environmental Stress Response (Shanxi Normal University) in Shanxi Province, Taiyuan, Shanxi, 030000, People's Republic of China*
[*]*Corresponding author's email: hhwrsl@163.com*

Abstract

Cerium–Nitrogen co–doped carbon quantum dots (Ce-N-CDs), a novel type of carbon-based nanomaterials, are prepared using hydrothermal synthesis. Ce-N-CDs demonstrate low toxicity, stability, and satisfactory biocompatibility. Effects of Ce-N-CDs on *Arabidopsis* root growth were analyzed at the molecular and physiological levels in this work. Ce-N-CDs (0.04 mg/mL) promoted the root tip meristem (RAM) and primary root (PR) growth. Ce-N-CDs effectively regulated the genes expression associated with cell cycle and facilitate the RAM and PR growth by enhancing cell division capacity of the RAM and activity of stem cells niche. The expression of auxin synthesis genes was upregulated after treatment with Ce-N-CDs, and the increased abundance of auxin transporters PIN1, PIN2, and PIN7 led to the increased accumulation of auxin and promotion of root growth. Thus, Ce-N-CDs can potentially promote plant growth and bioimaging.

Key words: Ce-N-CDs; Bioimaging; Auxin; Cell division; Gene expression.

Introduction

In recent years, on account of the raising production, the ecological effect of nano-materials diffusion in environment has aroused extend research attention (Batley *et al.*, 2013). Nanotechnology has become an important tool for increasing agricultural productivity. Molecular mechanisms by which nanoparticles respond in plants must be thoroughly considered because effects of nanoparticles on plant systems are remarkably more complex than expected. Carbon dots (CDs) are the nanomaterials based on carbon with characteristics of biocompatibility and minimal environmental toxicity due to their nontoxic carbon skeleton (Li *et al.*, 2019). Therefore, CDs are also often used as objects for investigating interactions with plants. For example, CDs can facilitate the mung bean roots growth, (Wang *et al.*, 2018; Zhang *et al.*, 2018) although other CDs suppress the plant roots growth (Chen *et al.*, 2016; Yan *et al.*, 2021). The CDs' conflicting effects against plants may be determined by the type of plant, stage of growth and development, and their own nature and concentration. Doping of heteroatoms (elements, such as Mg, La, and Ce) onto CDs can also enhance the distinctive optical performances of CDs in some practical applications (Zhang *et al.*, 2017; Han *et al.*, 2018; Zhang *et al.*, 2019). The incorporation of rare earth elements can exert a positive role on the growth of plant (Fashui, 2002; An *et al.*, 2020). However, high concentrations of lanthanum (La) and cerium (Ce) can present toxic effects against the growth of plant root (Zhang *et al.*, 2013). Cerium is a rich rare earth element containing high ecological value. However, studies on Ce typically focus on germination, biomass, and physiological effects of nanomaterials on plants. We chelated CDs and Ce into a novel nanomaterial to investigate physiological mechanisms of its interactions with plants thoroughly.

Terrestrial plants rely on their roots to absorb water and nutrients and transport them to various organs via the vascular bundle. Furthermore, roots provide support for the plant. The root system can respond to changes in the environment because of its direct contact with the external environment. Cell division and differentiation in the RAM contribute to the continuous growth of the root (Petricka *et al.*, 2012). The RAM is composed of four stem cells groups and a quiescent center (QC). QC cells divide very infrequently or even not at all (Van Den Berg *et al.*, 1997). The concentration of auxin in the course of root growth together with development is modulated through the two pathways of SCARECROW (SCR)/SHORT-ROOT (SHR) and PLETHORA1 (PLT1)-PIN auxin transport carriers (Ulmasov *et al.*, 1997; Aida *et al.*, 2004; Galinha *et al.*, 2007). However, Ce-N-CD regulation of root structure via the auxin pathway remains unclear.

Previous studies generally focused on oxidative stress of CDs on plants and photosynthesis (Li *et al.*, 2019; Xiao *et al.*, 2019; Chandrakar *et al.*, 2020; Chen *et al.*, 2020; Chen *et al.*, 2020). Therefore, in this work, *A. thaliana*, citric acid, ethylenediamine and cerium nitrate were respectively utilized as plant material, carbon source, nitrogen source, and doping material to integrate Ce–N co-doped CDs in quantum dots via hydrothermal synthesis. We then characterized the novel Ce-N-CDs, verified their biocompatibility, and investigated their application in phytology. The experimental results showed that Ce-N-CDs demonstrate low biotoxicity and can affect the cell cycle and auxin synthesis by entering roots of plants. Hence, we hypothesized that the application of Ce-N-CDs may potentially affect the growth together with development of plant root.

Experimental methods

Synthetic materials and characterization apparatus for Ce-N-CDs: The cerium nitrate, ethylenediamine, and citric acid were analytically pure and purchased from Shanxi Aiko Laboratory Equipment Co. Transmission electron microscope was employed for acquiring the images of high-resolution transmission electron microscopy and transmission electron microscopy images. Cary 300 UV–vis spectrophotometer was conducted to determine UV–visible spectra. With Nicolet 380 infrared spectrometer (Varian, USA), the fourier transform infrared (FTIR)

spectra could be acquired. The instrument of Thermo ESCALAB 250Xi was applied for measuring X-ray photoelectron spectroscopy (XPS). Fluorescence was measured using an LS-55 fluorescence spectrophotometer (Perkins Elmer, USA).

Synthesis of Ce-N-CDs: Ce-N-CDs and Ce-CDs were integrated utilizing a hydrothermal synthesis method. Citric acid (2 g) and $Ce(NO_3)_3$ (2 g) were dissolved in ultrapure water (40 mL) and ethylenediamine (1 mL) was next added when stirring prior to the mixture was dissolved fully. The mixture after dissolved was subsequently transferred into the lined autoclave and heated for 120 min under a temperature of 180°C. Cooling the sample to RT and centrifuging it (10,000 r/min, for 20 min) after heating. Supernatant was retained and sieved via a filtering device (0.22 mm) to generate an uniformly dispersed solution. Ultimately, the resulting solution was frozen in refrigerator for one day and subsequently dried utilizing vacuum freeze dryer to obtain dried Ce-N-CDs solids.

Cell toxicity test of Ce-N-CDs: Cell Counting Kit-8 (CCK-8) was employed for determining the Ce-N-CDs' cell toxicity (Cai *et al.*, 2019) HeLa cells were used in this study. The suspension of cell was added into a cell culture plate (96 well) and cultivated in a 5% CO_2 incubator under a temperature of 37°C for one day. Ce-N-CD solution containing a concentration between 0 and 0.7 mg/mL was produced with complete medium (90%DMEM+10%fetal serum) to continue the culture of cell for half a day, in which the concentration of the control group was 0 mg/ml. Cell survival rate was counted through the measurement of the absorbance of test hole with a microplate reader as follows: $VR = A / A_0 \times 100\%$, in which A and A_0 denote the cell absorbance with or without the probe treatment, respectively. Each measurement is repeated three times.

Plant culture: The plant used in this experiment is *A. thaliana* (Col-0, *DR5-GUS*, *PIN7:PIN7-GFP*, *PIN2:PIN2-GFP*, *PIN1:PIN1-GFP*, *CYCB1;1:CYCB1;1-GUS*, *QC25-GUS*, *WOX5:WOX5-GFP*). Seeds are first soaked for 1 hour and then placed in the refrigerator at 4°C for vernalization for 3 days. The surface of seed is disinfected through 1.5% (v/v) NaClO for ten minutes and next rinsed utilizing sterile water for 5 times. The seeds were cultivated on MS medium add with various concentrations of Ce-N-CDs. Samples were placed in a light incubator with a temperature of 22°C/18°C and cultured in a simulated photoperiod (16 h/8 h). Root length was measured with a ruler in the experiment. RAM is defined as the region from the rest center to the first significantly elongated cortical cell. The Image J software was implemented for determining RAM length.

Microscopy imaging: HeLa cell imaging: Add Ce-N-CD solution (10 μL) into the culture medium containing cultured HeLa cells and incubate under a temperature of 37°C for 120 minutes. Cells were cleaned for 3 times applying PBS buffer solution (10 mM, with a pH of 7.4), and Olympus laser confocal microscope was conducted for cell fluorescence imaging.

In vivo imaging of plants: The laser confocal microscope was employed for observing the distribution and absorption of Ce-N-CDs in the roots and *A. thaliana* leaves together with the GFP fluorescence. The excitation wavelength of Ce-N-CDs and GFP under laser confocal microscope are 405 nm and 488 nm, respectively. Image J software was implemented to quantify the GFP fluorescence intensity.

GUS staining: The GUS histochemical staining was carried out with root tip (Nan *et al.*, 2014). The transparency was utilized to treat root after staining at 37°C for 12 hours in dark environment. Stained pictures were then obtained on a fluorescence microscope (OLYMPUS, BX53). Finally, the activity of Gus was quantified (Béziat *et al.*, 2017).

RT-qPCR assay: Fresh root tips (approximately 0.5 cm) from each experimental group at 7 days of age were taken, quick frozen utilizing the liquid nitrogen, and placed under a temperature of −80°C. RNA could be extracted from the root tips employing the TRIzol method and cDNA strands were subsequently obtained via reverse transcription (TransScript One-Step gDNA Removal and cDNA Synthesis SuperMix, Transgen, China). The changes in relevant genes expression was determined through the instrument of real-time fluorescence quantitative PCR (ABI 7500Fast Real-Time PCR System, China). The comparative$2^{-\Delta\Delta Ct}$ approach was applied to count the relative genes expression (Livak & Schmittgen, 2001) *EF1α* was selected as an internal reference gene (Lilly *et al.*, 2011). Table 1 summarizes all the primer sequences in the current work.

Table 1. Primer sequences for qRT-PCR.

Gene name	Forward primer (5'-3')	Reverse primer (5'-3')
EF1α	CCAGGCTGATTGTGCTGTTCT	GGTGGTGGCATCCATCTTGTT
Histone 4	GATTCGTCGTCTTGCTCGTAG	CAGTCACCGTCTTCCTCCTC
CYCB1;1	CTCTTCTCATGTCGGCCAAGTA	GTCGGAACTGTCAAGTACCACTCA
CDKA;1	GGAAACCAACGGACCTAGAAACT	ATGCCTCCAAGATCCTTGAAGTAT
PCNA1	TTGGTGACACAGTTGTGATCTCTG	CTATCACAATTGCATCTTCCGG
PCNA2	CTCAGTAGCATTGGTGACACAGTTG	ACAGGCTCGTTCATCTCTATCACA
YUC3	CAACGTCCCTTCATGGCTTAA	TCTCGTGAACCCTACCGCATAC
YUC5	TCTGGCGCATCAAGACAACA	TCACCTCGCCTTCAAACTCC
YUC9	CTTGTCGTCGGATGTGGAAACT	GCCACTTCATCATCATCACTGAGAT
SUR1	TGGTGTGTGATAGGCTCAAGGA	ATCCATCAATGACAGCTCCAACTT
AAO3	TGGTAGCACGACATCCGAGAG	TGACCATACGCTTGTTGAATGAGT

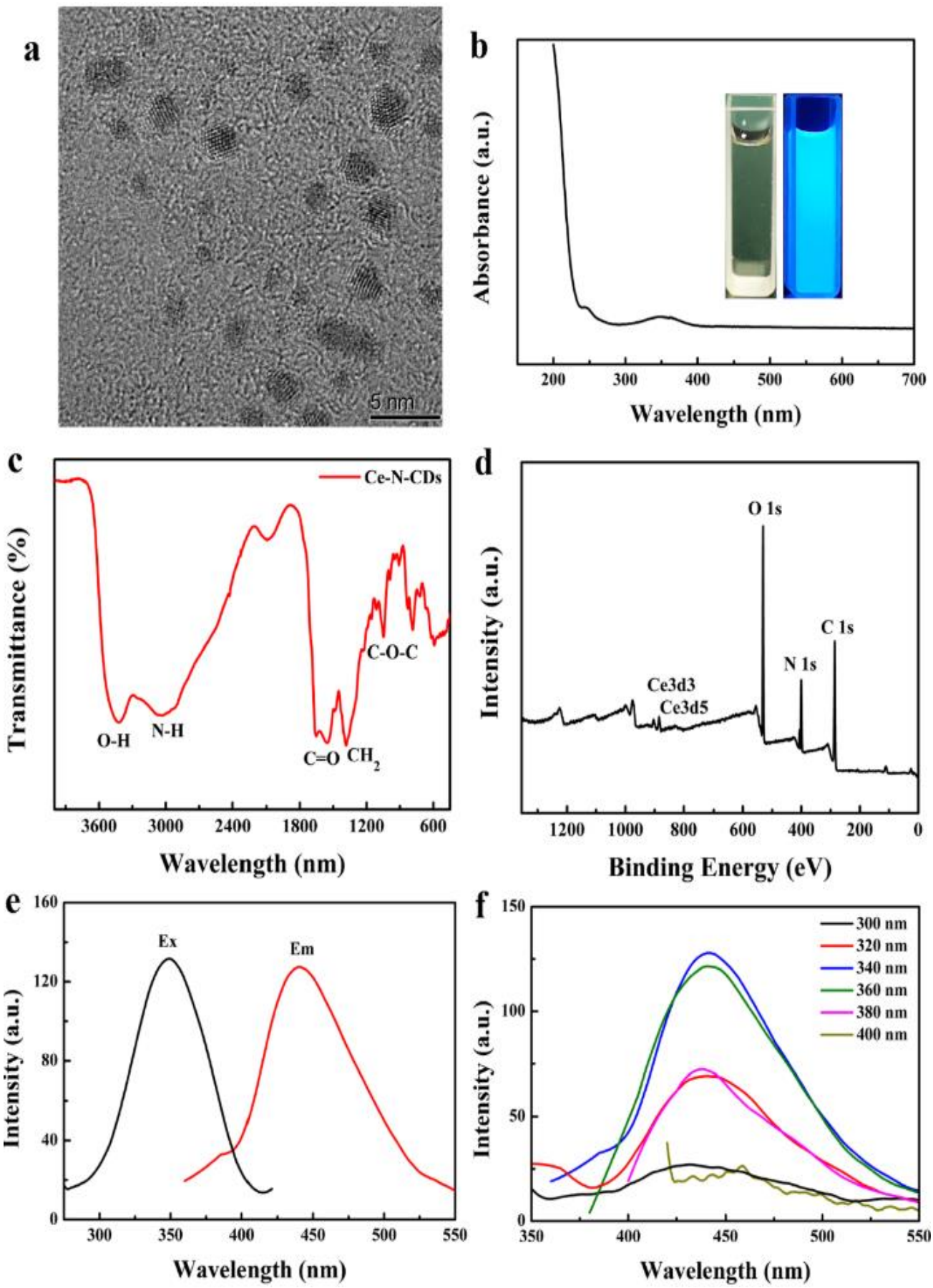

Fig. 1. (a) TEM of Ce-N-CDs. (b) and the ultraviolet-visible absorption spectra of the Ce-N-CDs. Inset: The diagram of the water Ce-N-CDs under UV light (340 nm) sunlight, respectively. (c) The FTIR spectra and (d)XPS spectra of the Ce-N-CDs. (e) Ce-N-CDs' emission and excitation spectra. (f) The emission spectra related to excitation of Ce-N-CDs at various excitation wavelengths.

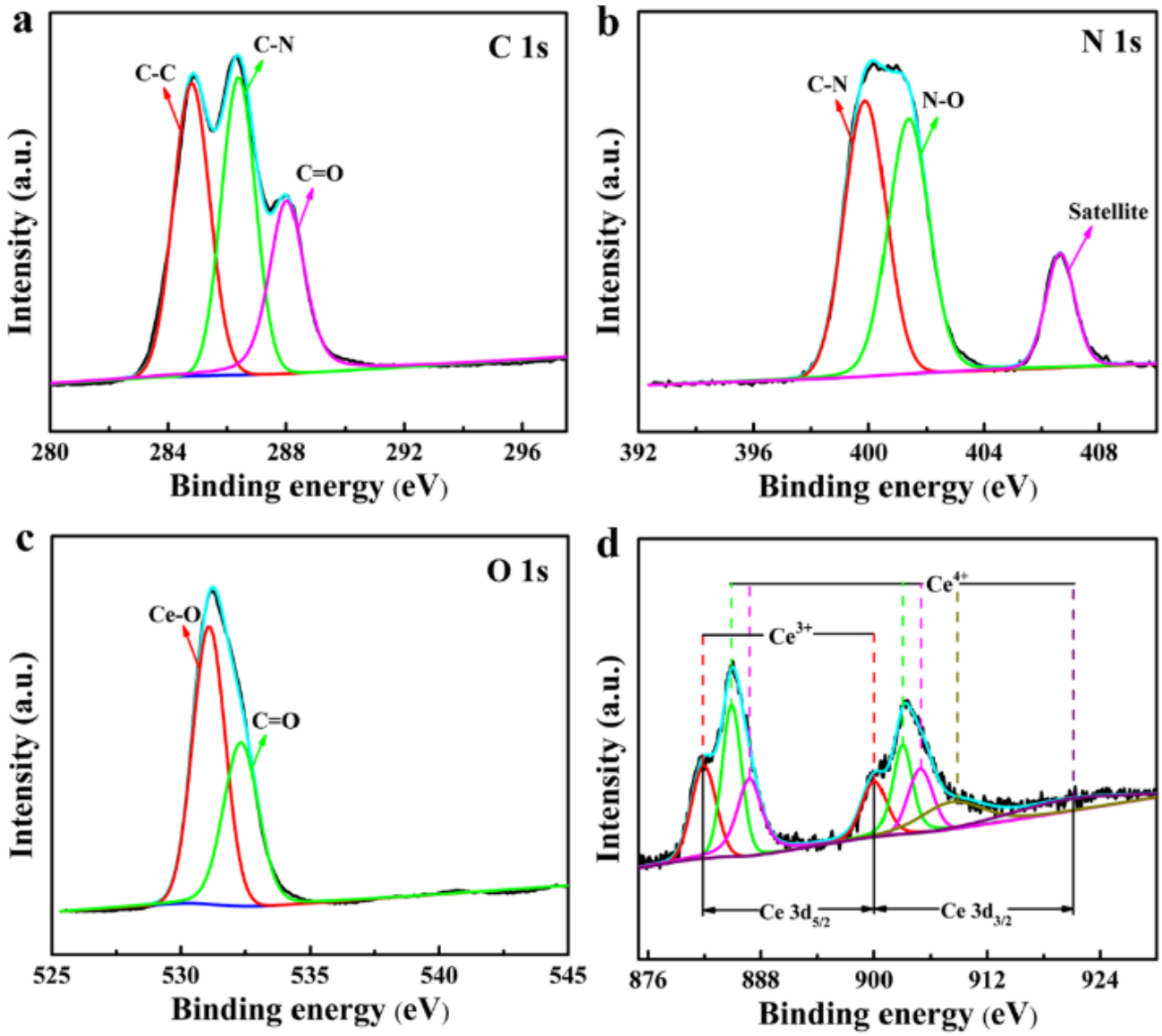

Fig. 2. Single element spectrogram of Ce-N-CDs. (a)Spectra of C 1s.(b) N 1s.(c) O 1s and (d) Ce 3d.

Statistical analysis

All the tests were repeated three times. The data of experiment were analyzed through one-way ANOVA on the basis of Newman Keuls multiple comparison detection ($P \leq 0.05$) Origin 8 and GraphPad Prism 5 were applied for mapping of data and statistical analysis.

Results and Analysis

Characterization and spectroscopic properties of Ce-N-CDs: The transmission electron microscopy (TEM) can be carried out to characterize the morphology of Ce-N-CDs. The TEM outcomes suggested that Ce-N-CDs are mostly spherical and properly dispersed (Fig. 1a). The ultraviolet absorption spectra of the Ce-N-CDs in Fig. 1b showed that an absorption peak is observed at 340 nm likely due to the n–π* electron leap (Atchudan *et al.*, 2017; Liu *et al.*, 2019). The inset in Fig. 1b based on the Ce-N-CDs water solution under sunlight and ultraviolet light (340 nm) revealed that under the ultraviolet excitation, the Ce-N-CDs can emit blue light. The infrared spectroscopy was applied to explore the chemical functional groups on the Ce-N-CDs surface (Fig. 1c). Peaks at 3,418 and 3,044 cm^{-1} are caused by contraction vibrations of N–H and O–H bonds. The tensile vibrations peaks of C=O bonds are presented at 1,555 and 1,653 cm−1, those at the CH_2 bond are observed at 1,376 cm^{-1}, and those at the C–O–C bond are exhibited at 1,222 and 1,043 cm^{-1}. The outcomes of FTIR reflected that the Ce-N-CDs surface involves hydrophilic groups, for instance unsaturated C–H, carboxyl, and hydroxyl groups, which lead to extremely water soluble and dispersible Ce-N-CDs. The elemental composition of the Ce-N-CDs surface was further analyzed via XPS. Fig. 1d shows that four peaks, namely, N1s (400 eV), C1s (285 eV), Ce3d (903 eV) and O1s (531 eV), contain nitrogen, carbon, cerium oxygen on the Ce-N-CDs surface. This finding corresponds to the results of the single element analysis through XPS (Fig. 2). The results clearly showed that the element Ce on the Ce-N-CDs surface is reflected in the form of Ce^{4+} and Ce^{3+}. The fluorescence spectrophotometer was utilized for determining the optical performances of Ce-N-CDs. Fig. 1e reveals the Ce-N-CDs' emission and excitation spectra. At 440 nm, Ce-N-CDs exhibit the

largest emission peak with 340 nm of excitation wavelength. Fig. 1f reflects the Ce-N-CDs' FL emission spectra with the excitation wavelengths between 300 nm and 400 nm. The outcomes exhibited that Ce-N-CDs' fluorescence performances are acceptable.

Biological toxicity of Ce-N-CDs and stability of fluorescence (FL) intensity: We measured the biological toxicity and fluorescence stability of Ce-N-CDs to detect their applicability to organisms. HeLa cells were selected in this study for measuring the cell toxicity. Seven concentrations of Ce-N-CDs were set and used to culture HeLa cells, respectively. The results in Fig. 3a showed that the cell survival rate is at least 95% with 0.4 mg/ml of Ce-N-CDs concentration. The cell survival rate was still exceed 85% with 0.7 mg/ml of Ce-N-CDs concentration. However, the concentration we used in the experiment was significantly less than 0.4 mg/ml. We tested the Ce-N-CDs' fluorescence stability at different pH values, ionic strengths, and times when the excitation wavelength was 340 nm (Fig. 3b–3d). The FL intensity of Ce-N-CDs fluctuates slightly and is stable when the pH value is 5.0–7.0 in different pH solutions (Fig. 3b). Therefore, the pH value of 5.0–7.0 is the optimal range of FL strength and selected for subsequent experiments in the current work. Ce-N-CDs were dissolved in NaCl solutions of different concentrations to test the Ce-N-CDs' FL stability at high concentration of salt, and the FL intensity was recorded (Fig. 3C). The results showed that the FL intensity is still unchanged basically with the concentration of NaCl between 0 M and 1.0 M. This finding indicated that the Ce-N-CDs' FL intensity remains unaffected by the change of salt concentration and presents satisfactory stability. Fig. 3d illustrates the effect of different times on FL strength in the PBS solution at pH 7.0. The results showed that the Ce-N-CDs' fluorescence remains unaffected by time and Ce-N-CDs exhibit low cell toxicity and fluorescence stability and can be used in subsequent biological-related experiments.

Absorption and distribution of Ce-N-CDs: Ce-N-CDs were incubated in animal and plant cells and then observed with a laser confocal microscope to explore their biocompatibility. First, HeLa cells were incubated with Ce-N-CDs for 3 hours. The change in cell morphology was insignificant although fluorescence signals can be detected and Ce-N-CDs entered cells and became enriched in the cell membrane and cytoplasm (Fig. 4). This finding suggested that Ce-N-CDs may play a role in cell cytoplasm and membrane.

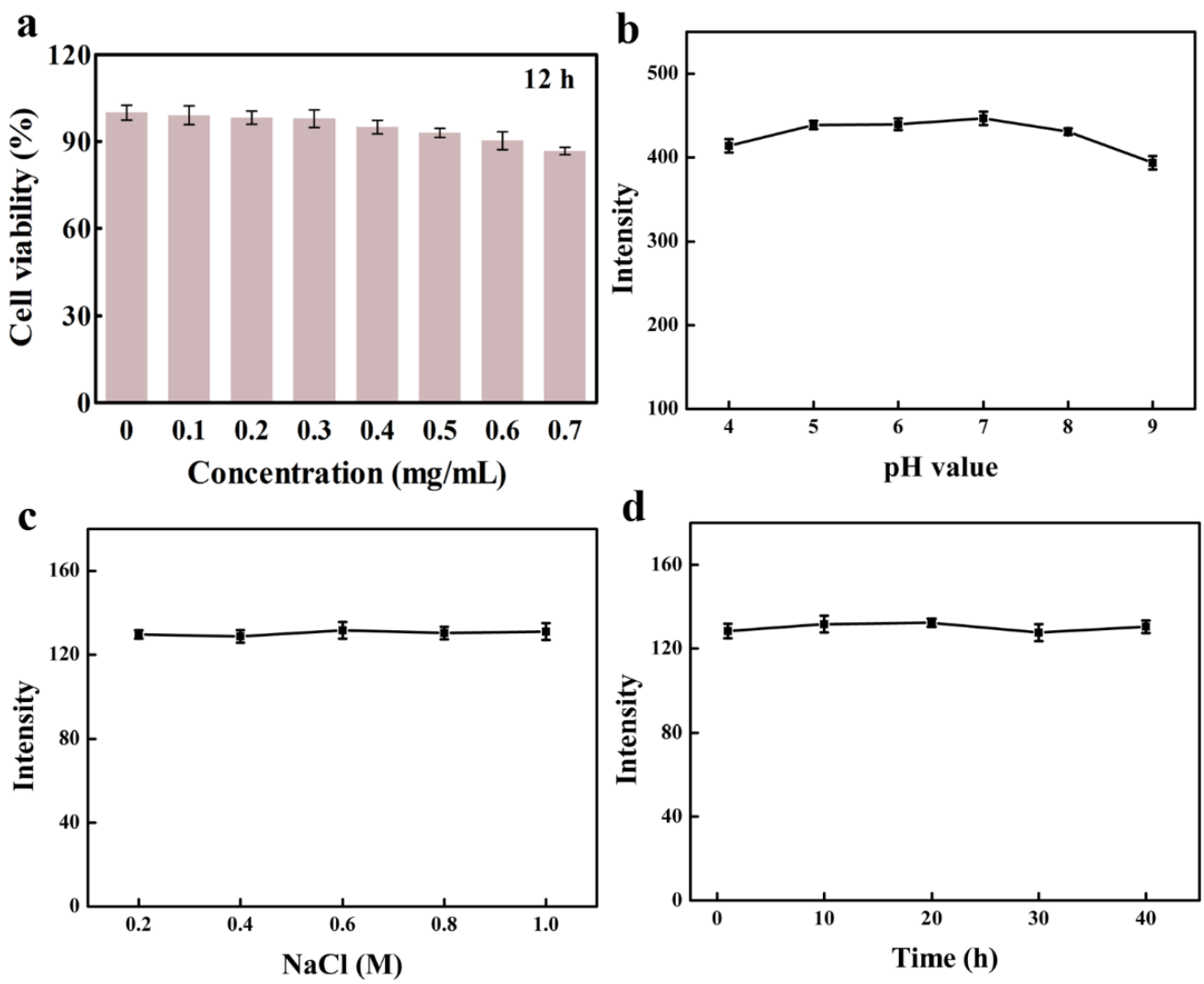

Fig. 3. (a) Cell viability of HeLa cell at different concentration of Ce-N-CDs for 12 h. Ce-N-CDs' FL Intensity at various pH value (b), concentrations of NaCl solution (c) and time (d).

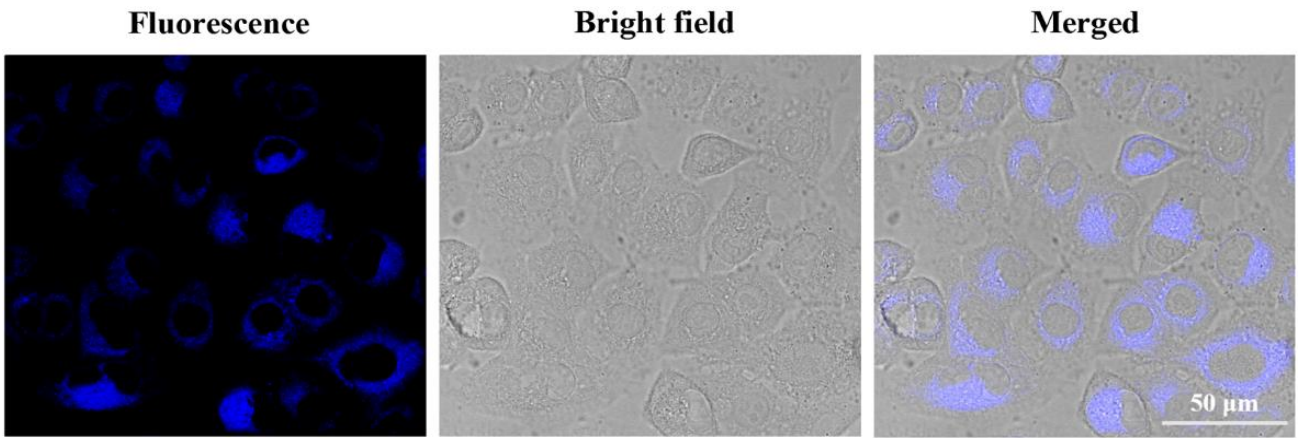

Fig. 4. Fluorescence imaging of Ce-N-CDs in HeLa cells.

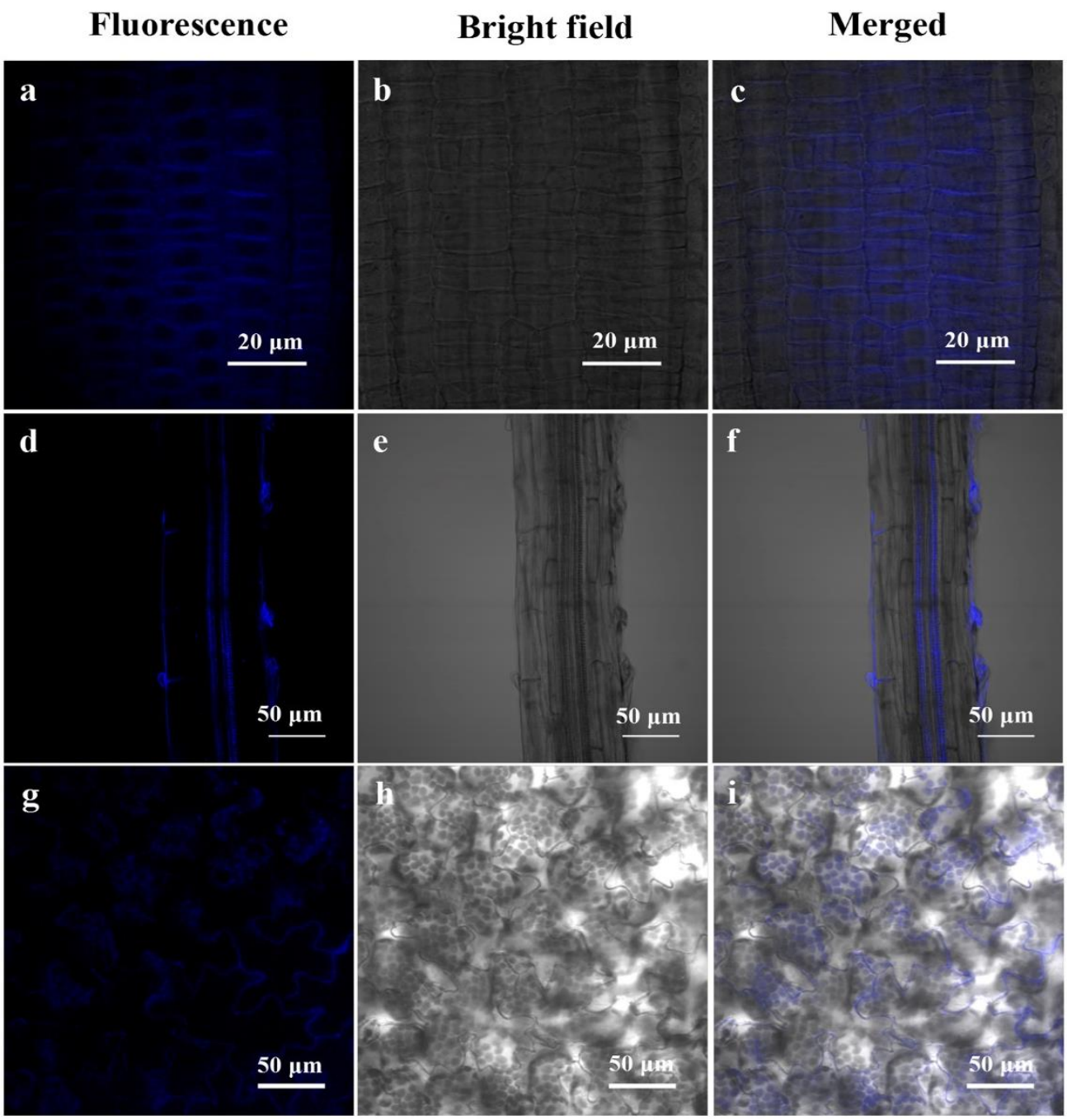

Fig. 5. The distribution and absorption of the Ce-N-CDs in *A. thaliana* seedlings.

In the RAM of *A. thaliana*, the fluorescence signals could be found, and the strong signals were found in the cell cytoplasm and membrane (Fig. 5a–5c). Furthermore, a large amount of blue fluorescence was also revealed in the mature area of the root, which is located in the vascular bundle (Fig. 5d–5f). Fluorescence signals can be detected in mesophyll cells and localized in chloroplasts because of their enrichment in cotyledons (Fig. 5g–5i). In conclusion, Ce-N-CDs can be absorbed by animal and plant cells and located in the cell membrane and cytoplasm. Particularly, fluorescent signals can also be detected in mesophyll cells of leaves in *A. thaliana*.

Previous studies showed that the uptake of CDs by *A. thaliana* cells is similar to that of animal cells and CDs can be absorbed into the cell cytoplasm and membrane for imaging (Cao *et al.*, 2007; Chen *et al.*, 2013; Tan *et al.*, 2013). However, carbon dots experience difficulty in entering the nucleus via cell membrane, and even those that enter nucleus require to be cultivated for a long time (Puvvada *et al.*, 2012). Different from animal cells, plant cells given that the cell wall of plant cells acts as a protective barrier that modulated the substances transport through stomata (Kurepa *et al.*, 2010; Ran *et al.*, 2010). Therefore, the absorption of Ce-N-CDs in the cell wall is mainly determined by the size of pores and particles on cell wall. Ce-N-CDs can pass through the pore size of the plant cell wall (about 10 nm) and then enter the cell for absorption because their volume is less than 5 nm (Fig. 1a). (Kruk *et al.*, 1999; Berestovsky *et al.*, 2001) Ce-N-CDs typically distributed in the cell cytoplasm and membrane are stained (Dong *et al.*, 2012; Zhang *et al.*, 2013). Plants absorb water and inorganic salts through apoplastic and symplastic pathways (Steudle & Peterson, 1998; Jackson *et al.*, 2000). Other studies have proven that CDs can enter the mung bean vascular bundle through the pathway of apoplast although fluorescence is absent in mung bean cells.(Li *et al.*, 2016) Chen (Chen *et al.*, 2018) hold that CDs are transported in *Arabidopsis* through the apoplastic pathway and demonstrated that Ce-N-CDs can enter the cytoplasm through the cell membrane and wall of root tip cells, thereby indicating that Ce-N-CDs entered *A. thaliana* in two ways. Therefore, tissue and subcellular localizations of Ce-N-CDs in *A. thaliana* based on laser confocal microscopy demonstrated the application potentiality of Ce-N-CDs in biological imaging.

Promotional effects of Ce-N-CDs on *A. thaliana* roots: *A. thaliana* seeds were seeded on the medium of MS added with Ce-N-CDs concentrations between 0 and 0.04 mg/mL for culture to investigate whether Ce-N-CDs can positively affect roots of *A. thaliana*. The phenotype of *A. thaliana* seedlings grown for 7 days (Fig. 6a) showed that Ce-N-CDs exert a promoting effect on roots. We then measured the primary roots length (Fig. 6b). The results clearly demonstrated that the primary roots length increased with increasing concentration when seedlings are grown for 7 days in the medium containing Ce-N-CDs. The length reaches the maximum at 0.04 mg/mL of concentration, which is a significant level and 11.9% longer than the control. The main root length followed the same trend as the incubation of 7 days when the incubation time was 8 days. Therefore, we conclude that Ce-N-CDs can promote root length. Finally, 0.04 mg/mL of concentration was chosen for subsequent experiments.

The RAM is the key factor of root elongation. We measured the RAM length from 5 days to 8 days to demonstrate whether the promotion of root growth by Ce-N-CDs is related to the RAM further (Fig. 6c). The RAM length was significantly higher by 20.6% after 7 days of treatment with Ce-N-CDs in contrast to the length of control. The results suggested that Ce-N-CDs can potentially influence cell division in the RAM to promote root growth.

Ce-N-CDs affect cell division: We demonstrate the impact of Ce-N-CDs against cell division in this section. GUS staining was applied to the *A. thaliana* transgenic line CYCB1;1-GUS in this experiment. *CYCB1;1* is a cell cycle protein and its expression is involved in the G2/M phase transition and activities indicative of cell division (Colón-Carmona *et al.*, 1999). The activity of cytokinesis was significantly higher at 5 days of treatment with Ce-N-CDs compared with that of the control (Fig. 7a and 7b). The growth continued for 2 days and the cytokinesis activity of the group treated with Ce-N-CD remained evidently higher in comparison with control group. This outcome revealed that Ce-N-CDs can indeed increase the activity of cell division in the root tip meristematic zone.

We performed relative quantification experiments on cell cycle- (*Histone 4*, *CYCB1;1*, and *CDKA;1*) and cell proliferation- (*PCNA1* and *PCNA2*) related genes using qRT-PCR to investigate changes in regulatory genes of the *A. thaliana* root tip cell cycle further. *Histone 4* is involved in the G1/S phase transition of the *Arabidopsis* cell cycle (Cui *et al.*, 2017). The relative *Histone 4* expression elevated by 78% compared with that of controls after treatment with Ce-N-CDs (Fig. 7c). *CYCB1;1* and *CDKA;1* are specifically expressed in the G2/M phase, (Doerner *et al.*, 1996; Shaul *et al.*, 1996; Cao *et al.*, 2018) and their relative expression elevated by 50% and 69%, respectively, compared with that of controls (Fig. 7c). *PCNA1* and *PCNA2* are cell proliferation marker genes (Cui *et al.*, 2017) and their relative expression elevated by 28% and 11%, respectively, compared with that of controls (Fig. 7c). For all the associated genes, the relative expression elevated in varying degrees after culture with Ce-N-CDs.

For the cell cycle marker genes, their relative expression in G2/M and G1/M phases significantly reduced and root growth was inhibited in a study of Cd stress on *A. thaliana* root growth (Cui *et al.*, 2017). Moreover, the promoter activity of CYCB1;1-GUS reduced under salt stress similar to the relative expression of *CYCB1;1* as well as the suppression of root growth (Burssens *et al.*, 2000). Ce-N-CDs raised the activity of cell division and the expression for all the genes associated with cell cycle was significantly higher in the present study. The proteins expression associated with cell cycle is precisely modulated at both the post-transcriptional and transcriptional levels. These proteins are generated rapidly and then degraded to ensure that cells can successfully enter the next cell cycle for division (Wan *et al.*, 2019). Therefore, we suggested that Ce-N-CDs drive the activity of cell division through modulating the genes associated with cell cycle and promoting the root growth.

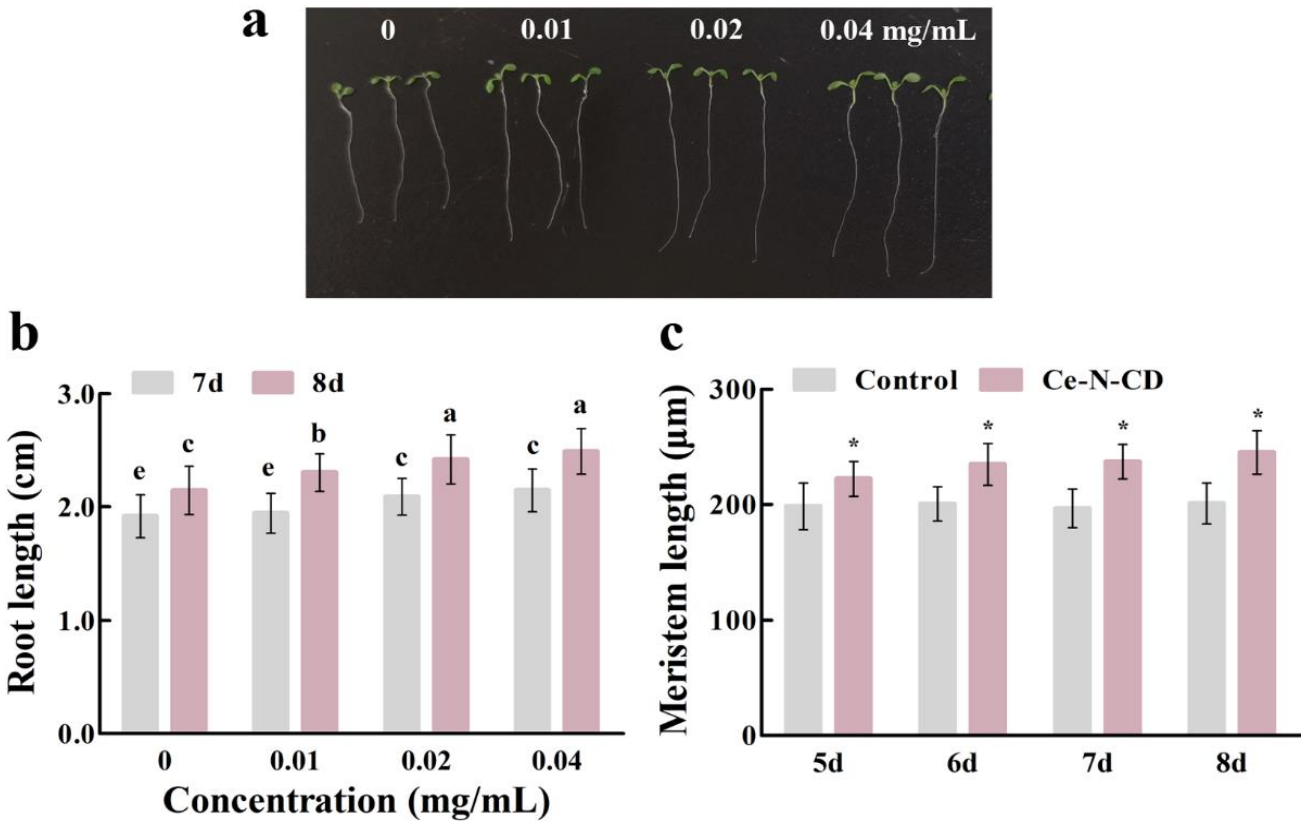

Fig. 6. Effects of Ce-N-CDs on root growth together with development of *A. thaliana*. (a) Phenotype of *A. thaliana* seedlings after 7 days of growth; (b) The length of *A. thaliana* root growing at 7 and 8 days; (c) Length of root apical meristem zone at 5-8 days of culture; Different letters denote evident differences ($p<0.05$). * represents significant difference between Ce-N-CDs treatment and control group ($p<0.05$).

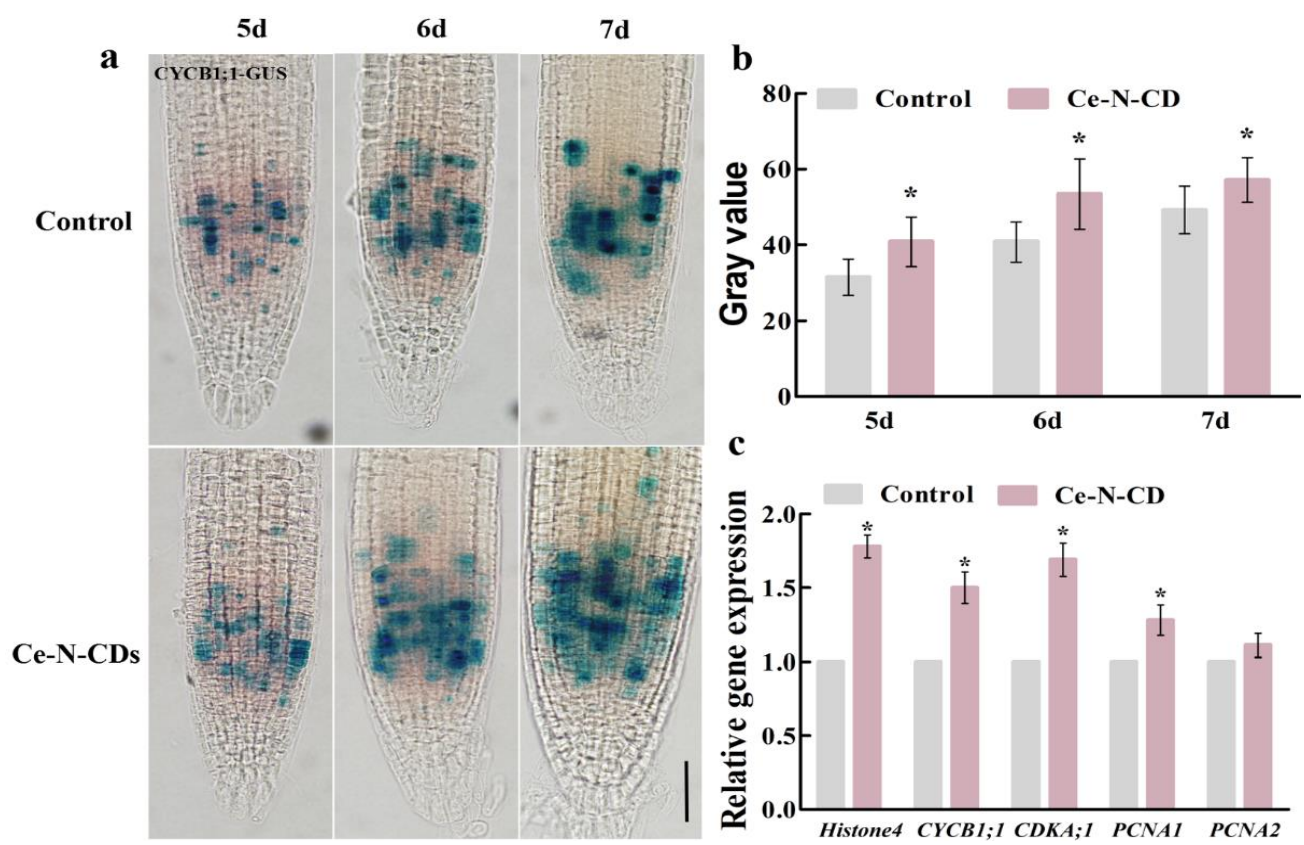

Fig. 7. Ce-N-CDs affects cell division in the meristem region of the root tip. (a) GUS staining images of transgenic line CYCB1;1-GUS at different times. (b) Quantitative activity of GUS. (c) The levels of relative genes expression levels related to cell cycle in *A. thaliana* treated with Ce-N-CDs for 7 days. * represents significant difference between control and Ce-N-CDs treatment group ($p<0.05$). Scale bar: 50 μm.

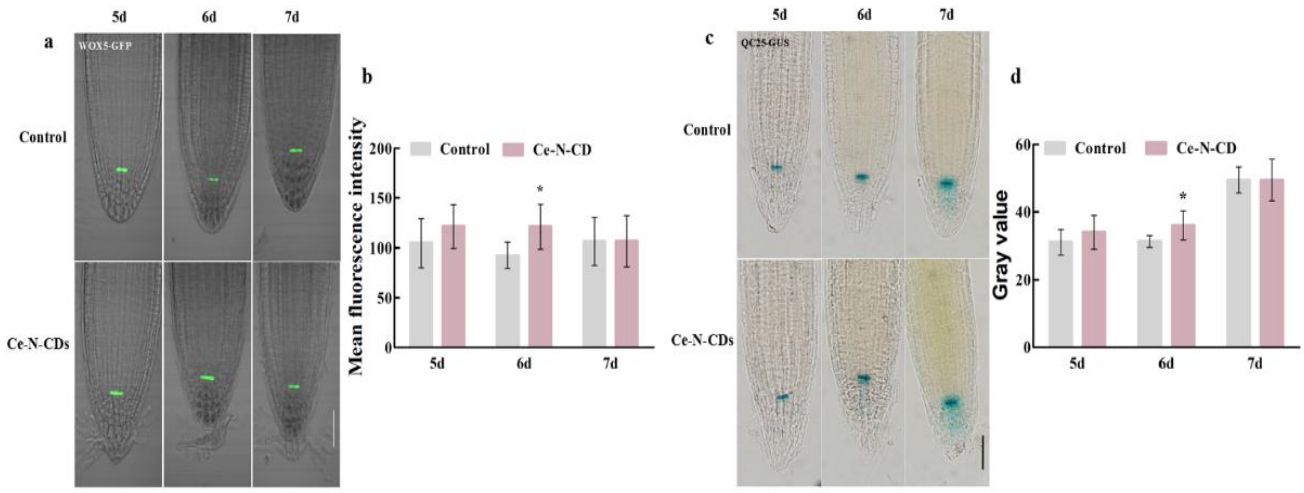

Fig. 8. Changes in stem cell niche activity after Ce-N-CDs treatment in *A. thaliana* root tip. (a) Changes of WOX5-GFP after Ce-N-CDs treatment. (b) fluorescence intensity of WOX5-GFP. (c) GUS staining image of QC25-GUS. (d) GUS activity quantification of QC25-GUS. * represents significant difference between control group and Ce-N-CDs treatment ($p<0.05$). Scale bar: 50 μm

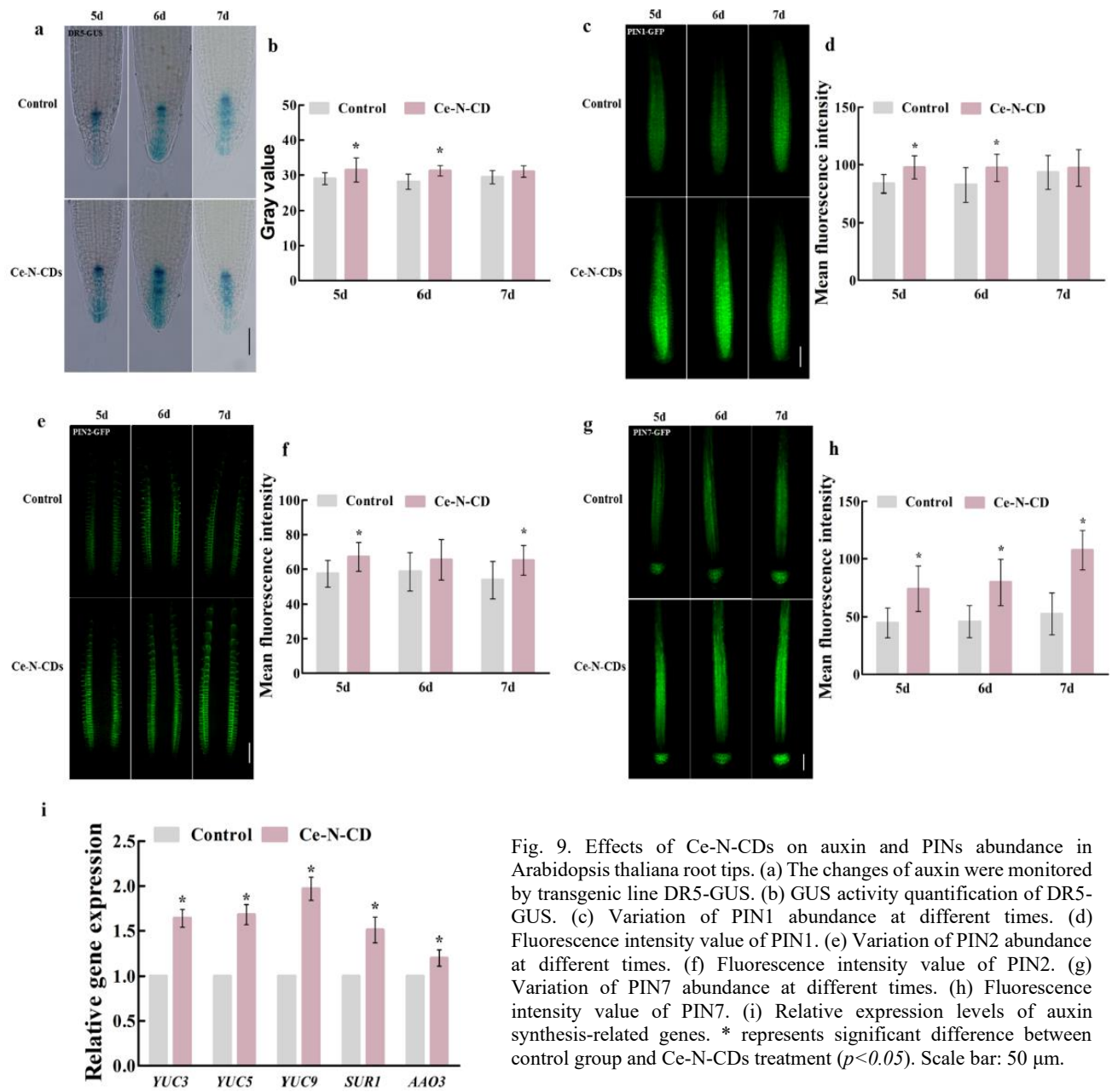

Fig. 9. Effects of Ce-N-CDs on auxin and PINs abundance in Arabidopsis thaliana root tips. (a) The changes of auxin were monitored by transgenic line DR5-GUS. (b) GUS activity quantification of DR5-GUS. (c) Variation of PIN1 abundance at different times. (d) Fluorescence intensity value of PIN1. (e) Variation of PIN2 abundance at different times. (f) Fluorescence intensity value of PIN2. (g) Variation of PIN7 abundance at different times. (h) Fluorescence intensity value of PIN7. (i) Relative expression levels of auxin synthesis-related genes. * represents significant difference between control group and Ce-N-CDs treatment ($p<0.05$). Scale bar: 50 μm.

Ce-N-CDs enhance the activity of stem cell niche of *A. thaliana* in root tip: We assayed the stem cell niche activity using two QC transgenic lines, namely, QC25-GUS and WOX5-GFP, to assess whether Ce-N-CDs affect the niche activity of *A. thaliana* root tip stem cell. The GFP fluorescence intensity and GUS activity of Ce-N-CD-treated WOX5-GFP (Fig. 8a and 8b) and QC25-GUS (Fig. 8c and 8d) root tips were both obviously higher in comparison with control at day 6. Both GUS and GFP signals were not evidently different from the signals in control group and approached normal levels at days 5 and 7. These outcomes suggested that Ce-N-CDs raised the meristematic zone length through improving the stem cell niche activity in root tip.

Altered accumulation of auxin and localization of PIN protein after Ce-N-CD treatment: Auxin exerts an essential effect through extensively regulating plant growth together with its development through its dynamic and differential distribution in plant tissues.(Vanneste & Friml, 2009) We investigate whether the mechanism by which Ce-N-CDs promote root length is related to auxin in this section. Therefore, DR5-GUS, the *A. thaliana* transgenic line was employed for evaluating the distribution or/and response to the auxin (Ulmasov *et al.*, 1997). We first examined changes in auxin after treatment with Ce-N-CDs using DR5-GUS. The results showed that the DR5-GUS promoter activity was significantly increased after 5 and 6 days of Ce-N-CD treatment compared with the control, and the concentration of auxin increased because the promoter activity was induced by auxin (Fig. 9a and 9b). Auxin accumulation returned to levels consistent with those of the control at 7 days of treatment.

The Ce-N-CD treatment effect against the auxin generation genes expression was further explored. Experiments were performed on the genes expression associated with auxin synthesis employing qRT-PCR. YUCCA (YUC) protein is required for auxin biosynthesis during plant development (Mashiguchi *et al.*, 2011). Transcript levels of *YUC* (*YUC3*, *YUC5*, and *YUC9*) were significantly higher after treatment with Ce-N-CDs compared with those of controls (Fig. 9i). *YUC3* and *YUC5* genes are responsible for auxin biosynthesis in roots and are highly expressed. Simultaneous silencing of *YUC9*, *YUC8*, *YUC7*, *YUC5*, and *YUC3* (*yucQ* mutants) led to the blockage of auxin synthesis in roots that ultimately suppressed the growth together with development of primary and lateral roots. Even excessive above-ground auxin synthesis fails to restore this phenomenon; meanwhile, the partial restoration of the root-deficient phenotype of the *yucQ* mutant through the application of exogenous auxin suggested that only auxin synthesized in root exerts a principal effect in the root development process (Chen *et al.*, 2014). Two other genes expression associated with auxin synthesis, namely, *SUR1* and *AAO3*, was also upregulated to significant levels compared with that of the control (Fig. 9i). This phenomenon may explain why the addition of Ce-N-CDs regulated the genes expression related to auxin, induced auxin synthesis, and increased auxin concentrations.

The distribution of root apical auxin is regulated by auxin transport carriers (Santelia *et al.*, 2008). PIN proteins in these transport carriers are a class of proteins essential in the polar transport of auxin (Wisniewska *et al.*, 2006). We used auxin transport carriers PIN7:PIN7-GFP, PIN2:PIN2-GFP, and PIN1:PIN1-GFP to investigate whether PIN transport carriers are stimulated by Ce-N-CDs to change and detect the expression of auxin carriers. The outcomes reflected that the fluorescence signal intensity of PIN1-GFP is markedly enhanced after 5–6 d of treatment with Ce-N-CDs and returns to a level consistent with that of the control by day 7 (Fig. 9c and 9d). However, the fluorescence signal intensity of PIN2-GFP was significantly enhanced at days 5 and 7 of treatment with Ce-N-CDs (Fig. 9e and 9f). The significantly higher abundance of PIN7-GFP at 5 d of treatment continued for two more days compared with that of the control (Fig. 9g and 9h). Low concentrations of single-walled carbon nanohorn (SWCNH) promote the *A. thaliana YUC5* and *YUC3* expression and increase the intensity of PIN2 expression to promote root growth (Sun *et al.*, 2020). Furthermore, the inhibition of *A. thaliana* roots under cadmium stress is caused by the reduction of auxin synthesis on account of the reduced abundance of PIN7, PIN3, and PIN1 proteins (Yuan & Huang, 2016). The maintenance of auxin polar transport is achieved through PINs, which play an integral role in maintaining RAM and root growth (Grieneisen *et al.*, 2007). On the basis of our outcomes, it can be summarized that Ce-N-CDs can increase the abundance of PINs to influence the distribution of auxin, induce auxin biosynthesis, and increase auxin accumulation in roots to facilitate the primary root growth. Taken together, these outcomes can give new insights into the molecular mechanisms modulated via Ce-N-CDs in the root tip.

Conclusion

Soluble Ce-N-CDs integrated via hydrothermal synthesis demonstrate low biological toxicity and stability, potential applicability in imaging, and suitability in membrane and cytoplasm imaging. Ce-N-CDs promote the root apical meristem growth by driving the cell cycle and auxin synthesis and transport to advance root growth. However, the role of Ce-N-CDs in plants requires further investigation at biochemical and molecular levels.

Acknowledgement

This work was supported by the Graduate innovation project of Shanxi Normal University (NO. 2019XBY017).

Reference

Aida, M., D. Beis, R. Heidstra, V. Willemsen, I. Blilou, C. Galinha, L. Nussaume, Y.S. Noh, R. Amasino and B. Scheres. 2004. The plethora genes mediate patterning of the *Arabidopsis* root stem cell niche. *Cell*, 119(1): 109-120.

An, J., P. Hu, F. Li, H. Wu, Y. Shen, J.C. White, X. Tian, Z. Li and J.P. Giraldo. 2020. Emerging investigator series: Molecular mechanisms of plant salinity stress tolerance improvement by seed priming with cerium oxide nanoparticles. *Environ. Sci. Nano.*, 7.DOI:10.1039/D0EN00387E.

Atchudan, R., T.N.J.I. Edison, D. Chakradhar, S. Perumal, J.J. Shim and Y.R. Lee. 2017. Facile green synthesis of nitrogen-doped carbon dots using chionanthus retusus fruit extract and investigation of their suitability for metal ion sensing and biological applications. *Sens Actuators B Chem.*, 246: 497-509.

Batley, G.E., J.K. Kirby and M.J. McLaughlin. 2013. Fate and risks of nanomaterials in aquatic and terrestrial environments. *Acc. Chem. Res*., 46(3): 854-862.

Berestovsky, G.N., V.I. Ternovsky and A.A. Kataev. 2001. Through pore diameter in the cell wall of chara corallina. *J. Exp. Bot*., 52(359): 1173-1177.

Béziat, C., J. Kleine-Vehn and E. Feraru. 2017. Histochemical staining of β-glucuronidase and its spatial quantification. *Methods Mol. Biol.*, 1497: 73-80.

Burssens, S., K. Himanen, B. Van de Cotte, T. Beeckman, M. Van Montagu, D. Inzé and N. Verbruggen. 2000. Expression of cell cycle regulatory genes and morphological alterations in response to salt stress in *Arabidopsis thaliana*. *Planta,* 211(5): 632-640.

Cai, L., X. Qin, Z. Xu, Y. Song, H. Jiang, Y. Wu, H. Ruan and J. Chen. 2019. Comparison of cytotoxicity evaluation of anticancer drugs between real-time cell analysis and cck-8 method. *ACS Omega*, 4(7): 12036-12042.

Cao, L., X. Wang, M.J. Meziani, F. Lu, H. Wang, P.G. Luo, Y. Lin, B.A. Harruff, L.M. Veca and D. Murray. 2007. Carbon dots for multiphoton bioimaging. *J. Amer. Chem. Soc.*, 129(37): 11318-11319.

Cao, X., H. Wang, D. Zhuang, H. Zhu, Y. Du, Z. Cheng, W. Cui, H.J. Rogers, Q. Zhang and C. Jia. 2018. Roles of MSH2 and MSH6 in cadmium-induced G2/M checkpoint arrest in *Arabidopsis* roots. *Chemosphere*, 201: 586-594.

Chandrakar, V., B. Yadu, J. Korram, M.L. Satnami, A. Dubey, M. Kumar and S. Keshavkant. 2020. Carbon dot induces tolerance to arsenic by regulating arsenic uptake, reactive oxygen species detoxification and defense-related gene expression in *Cicer arietinum* L. *Plant Physiol. Bioch.*, 156: 78-86.

Chen, B., F. Li, S. Li, W. Weng, H. Guo, T. Guo, X. Zhang, Y. Chen, T. Huang and X. Hong. 2013. Large scale synthesis of photoluminescent carbon nanodots and their application for bioimaging. *Nanoscale*, 5(5): 1967-1971.

Chen, J., R. Dou, Z. Yang, X. Wang, C. Mao, X. Gao and L. Wang. 2016. The effect and fate of water-soluble carbon nanodots in maize (*Zea mays* L.). *Nanotoxicology*, 10(6): 818-828.

Chen, J., B. Liu, Z. Yang, J. Qu, H. Xun, R. Dou, X. Gao and L. Wang. 2018. Phenotypic, transcriptional, physiological and metabolic responses to carbon nanodot exposure in *Arabidopsis thaliana* (L.). *Environ. Sci. Nano*., 5(11): 2672-2685.

Chen, Q., X. Dai, H. De-Paoli, Y. Cheng, Y. Takebayashi, H. Kasahara, Y. Kamiya and Y. Zhao. 2014. Auxin overproduction in shoots cannot rescue auxin deficiencies in *Arabidopsis* roots. *Plant Cell Physiol.*, 55(6): 1072-1079.

Chen, Q., B. Liu, H. Man, L. Chen, X. Wang, J. Tu, Z. Guo, G. Jin, J. Lou and L. Ci. 2020. Enhanced bioaccumulation efficiency and tolerance for Cd (II) in *Arabidopsis thaliana* by amphoteric nitrogen-doped carbon dots. *Ecotoxicol. Environ. Safe.*, 190: 110108.

Chen, Q., H. Man, L. Zhu, Z. Guo and L. Ci. 2020. Enhanced plant antioxidant capacity and biodegradation of phenol by immobilizing peroxidase on amphoteric nitrogen-doped carbon dots. *Catal Commun.*, 134: 105847.

Colón-Carmona, A., R. You, T. Haimovitch-Gal and P. Doerner. 1999. Spatio-temporal analysis of mitotic activity with a labile cyclin–gus fusion protein. *Plant J.*, 20(4): 503-508.

Cui, W., H. Wang, J. Song, X. Cao, H.J. Rogers, D. Francis, C. Jia, L. Sun, M. Hou and Y. Yang. 2017. Cell cycle arrest mediated by Cd-induced DNA damage in *Arabidopsis* root tips. *Ecotoxicol. Environ. Safe.*, 145: 569-574.

Doerner, P., J.E. Jørgensen, R. You, J. Steppuhn and C. Lamb. 1996. Control of root growth and development by cyclin expression. *Nature*, 380(6574): 520-523.

Dong, Y., C. Chen, X. Zheng, L. Gao, Z. Cui, H. Yang, C. Guo, Y. Chi and C.M. Li. 2012. One-step and high yield simultaneous preparation of single- and multi-layer graphene quantum dots from cx-72 carbon black. *J. Mater. Chem.*, 22(18): 8764-8766.

Fashui, H. 2002. Study on the mechanism of cerium nitrate effects on germination of aged rice seed. *Biol. Trace Elem. Res*., 87(1): 191-200.

Galinha, C., H. Hofhuis, M. Luijten, V. Willemsen, I. Blilou, R. Heidstra and B. Scheres. 2007. Plethora proteins as dose-dependent master regulators of arabidopsis root development. *Nature*, 449(7165): 1053-1057.

Grieneisen, V.A., J. Xu, A.F. Marée, P. Hogeweg and B. Scheres. 2007. Auxin transport is sufficient to generate a maximum and gradient guiding root growth. *Nature*, 449(7165): 1008-1013.

Han, Y., Y. Chen, N. Wang and Z. He. 2018. Magnesium doped carbon quantum dots synthesized by mechanical ball milling and displayed Fe^{3+} sensing. *Mater. Technol.*, 34(6): 336-342.

Jackson, R.B., J.S. Sperry and T.E. Dawson. 2000. Root water uptake and transport: Using physiological processes in global predictions. *Trends Plant Sci.*, 5(11): 482-488.

Kruk, M., M. Jaroniec and K.P. Gadkaree. 1999. Determination of the specific surface area and the pore size of microporous carbons from adsorption potential distributions. *Langmuir*, 15(4): 179-182.

Kurepa, J., T. Paunesku, S. Vogt, H. Arora, B.M. Rabatic, J. Lu, M.B. Wanzer, G.E. Woloschak and J.A. Smalle. 2010. Uptake and distribution of ultrasmall anatase tio2 alizarin red s nanoconjugates in *Arabidopsis thaliana*. *Nano lett.*, 10(7): 2296-2302.

Li, H., J. Huang, Y. Liu, F. Lu, J. Zhong, Y. Wang, S. Li, Y. Lifshitz, S.T. Lee and Z. Kang. 2019. Enhanced rubisco activity and promoted dicotyledons growth with degradable carbon dots. *Nano Res.*, 12(7): 1585-1593.

Li, W., Y. Zheng, H. Zhang, Z. Liu, W. Su, S. Chen, Y. Liu, J. Zhuang and B. Lei. 2016. Phytotoxicity, uptake, and translocation of fluorescent carbon dots in mung bean plants. *ACS Applied Mater Interfaces*, 8(31): 19939-19945.

Lilly, S., R. Drummond, M. Pearson and R. MacDiarmid. 2011. Identification and validation of reference genes for normalization of transcripts from virus-infected *Arabidopsis thaliana*. *Mol. Plant Microb. Interact*., 24(3): 294-304.

Liu, S., J. Cui, J. Huang, B. Tian, F. Jia and Z. Wang. 2019. Facile one-pot synthesis of highly fluorescent nitrogen-doped carbon dots by mild hydrothermal method and their applications in detection of Cr (VI) ions. *Spectrochimica Acta Part A: Mol. Biomol. Spectrosc.*, 206: 65-71.

Livak, K.J. and T.D. Schmittgen. 2001. Analysis of relative gene expression data using real-time quantitative pcr and the $2^{-\Delta\Delta CT}$ method. *Methods*, 25(4): 402-408.

Mashiguchi, K., K. Tanaka, T. Sakai, S. Sugawara, H. Kawaide, M. Natsume, A. Hanada, T. Yaeno, K. Shirasu and H. Yao. 2011. The main auxin biosynthesis pathway in *Arabidopsis*. *PNAS.*, 108(45): 18512-18517.

Nan, W., X. Wang, L. Yang, Y. Hu, Y. Wei, X. Liang, L. Mao and Y. Bi. 2014. Cyclic gmp is involved in auxin signalling during *Arabidopsis* root growth and development. *J. Exp. Bot*., 65(6): 1571-1583.

Petricka, J.J., C.M. Winter and P.N. Benfey. 2012. Control of *Arabidopsis* root development. *Ann. Rev. Plant Biol.*, 63: 563-590.

Puvvada, N., B.P. Kumar, S. Konar, H. Kalita, M. Mandal and A. Pathak. 2012. Synthesis of biocompatible multicolor luminescent carbon dots for bioimaging applications. *Sci. Technol. Adv. Mater.*, 13(4): 045008.

Ran, C., T.A. Ratnikova, M.B. Stone, S. Lin, M. Lard, G. Huang, J.S. Hudson and P.C. Ke. 2010. Differential uptake of carbon

nanoparticles by plant and mammalian cells. *Nano Micro Small*, 6(5): 612-617.

Santelia, D., S. Henrichs, V. Vincenzetti, M. Sauer, L. Bigler, M. Klein, A. Bailly, Y. Lee, J. Friml and M. Geisler. 2008. Flavonoids redirect pin-mediated polar auxin fluxes during root gravitropic responses. *J. Biol. Chem.*, 283(45): 31218-31226.

Shaul, O., V. Mironov, S. Burssens, M. Van Montagu and D. Inze. 1996. Two *Arabidopsis* cyclin promoters mediate distinctive transcriptional oscillation in synchronized tobacco by-2 cells. *PNAS.*, 93(10): 4868-4872.

Steudle, E. and C.A. Peterson. 1998. How does water get through roots? *J. Exp. Bot.*, 49(322): 775-788.

Sun, L., R. Wang, Q. Ju and J. Xu. 2020. Physiological, metabolic, and transcriptomic analyses reveal the responses of *Arabidopsis* seedlings to carbon nanohorns. *Environ. Sci. Technol.*, 54(7): 4409-4420.

Tan, M., L. Zhang, R. Tang, X. Song, Y. Li, H. Wu, Y. Wang, G. Lv, W. Liu and X. Ma. 2013. Enhanced photoluminescence and characterization of multicolor carbon dots using plant soot as a carbon source. *Talanta*, 115: 950-956.

Ulmasov, T., J. Murfett, G. Hagen and T.J. Guilfoyle. 1997. Aux/iaa proteins repress expression of reporter genes containing natural and highly active synthetic auxin response elements. *Plant Cell*, 9(11): 1963-1971.

Van Den Berg, C., V. Willemsen, G. Hendriks, P. Weisbeek and B. Scheres. 1997. Short-range control of cell differentiation in the *Arabidopsis* root meristem. *Nature*, 390(6657): 287-289.

Vanneste, S. and J. Friml. 2009. Auxin: A trigger for change in plant development. *Cell*, 136(6): 1005-1016.

Wan, J., R. Wang, R. Wang, Q. Ju, Y. Wang and J. Xu. 2019. Comparative physiological and transcriptomic analyses reveal the toxic effects of ZnO nanoparticles on plant growth. *Environ. Sci. Technol*., 53(8): 4235-4244.

Wang, H., M. Zhang, Y. Song, L. Hao, H. Hui, M. Shao, L. Yang and Z. Kang. 2018. Carbon dots promote the growth and photosynthesis of mung bean sprouts. *Carbon*, 136: 94-102.

Wisniewska, J., J. Xu, D. Seifertová, P.B. Brewer, K. Ruzicka, I. Blilou, D. Rouquié, E. Benková, B. Scheres and J. Friml. 2006. Polar pin localization directs auxin flow in plants. *Science*, 312(5775): 883-883.

Xiao, L., H. Guo, S. Wang, J. Li, Y. Wang and B. Xing. 2019. Carbon dots alleviate the toxicity of cadmium ions (Cd^{2+}) toward wheat seedlings. *Environ. Sci. Nano*., 6(5): 1493-1506.

Yan, X., Q. Xu, D. Li, J. Wang and R. Han. 2021. Carbon dots inhibit root growth by disrupting auxin biosynthesis and transport in *Arabidopsis*. *Ecotoxicol. Environ. Safe*., 216: 112168.

Yuan, H.M. and X. Huang. 2016. Inhibition of root meristem growth by cadmium involves nitric oxide-mediated repression of auxin accumulation and signalling in *Arabidopsis*. *Plant Cell Environ.*, 39(1): 120-135.

Zhang, C., Q. Li, M. Zhang, N. Zhang and M. Li. 2013. Effects of rare earth elements on growth and metabolism of medicinal plants. *Acta Pharm. Sin. B.*, 3(1): 20-24.

Zhang, L., Q. Yin, H. Huang and B. Wang. 2013. Conjugation of cationic poly (p-phenylene ethynylene) with dendritic; polyethylene enables live-cell imaging. *J. Mater. Chem. B.*, 1(6): 756-761.

Zhang, M., L. Hu, H. Wang, Y. Song, Y. Liu, H. Li, M. Shao, H. Huang and Z. Kang. 2018. One-step hydrothermal synthesis of chiral carbon dots and their effects on mung bean plant growth. *Nanoscale*, 10(26): 12734-12742.

Zhang, M., W. Wang, P. Yuan, C. Chi, J. Zhang and N. Zhou. 2017. Synthesis of lanthanum doped carbon dots for detection of mercury ion, multi-color imaging of cells and tissue, and bacteriostasis. *Chem. Eng. J*., 330: 1137-1147.

Zhang, M., L. Zhao, F. Du, Y. Wu, R. Cai, L. Xu, H. Jin, S. Zou, A. Gong and F. Du. 2019. Facile synthesis of cerium-doped carbon quantum dots as highly efficient antioxidant for free radical scavenging. *Nanotechnology*, 30(32): 325101.

(Received for publication 15 June 2024)